IEEE Photonics Journal
An IEEE Photonics Society Publication

Open Access

Broadband and Compact TE-Pass Polarizer Based on Hybrid Plasmonic Grating on LNOI Platform

Volume 13, Number 1, February 2021

Shuangxing Dai
Wenqi Yu
Yiru Zhao
Mingxuan Li
Jinye Li
Zhike Zhang
Jianguo Liu, ***Member, IEEE***

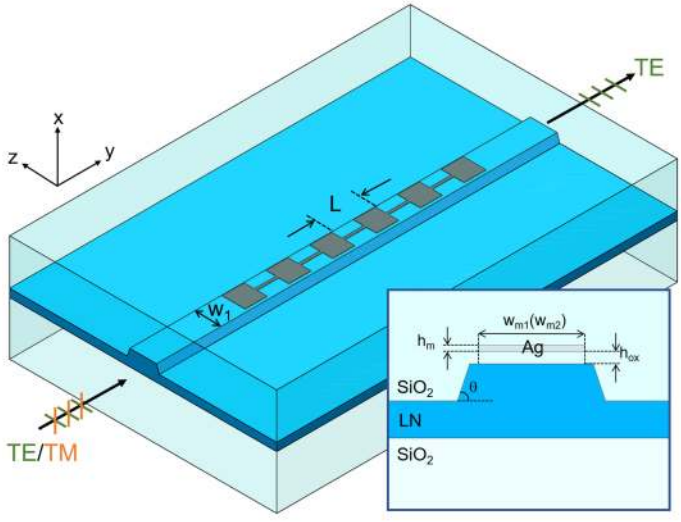

DOI: 10.1109/JPHOT.2020.3041286

Broadband and Compact TE-Pass Polarizer Based on Hybrid Plasmonic Grating on LNOI Platform

Shuangxing Dai,[1,2] **Wenqi Yu**,[1,2] **Yiru Zhao**,[1,2] **Mingxuan Li**,[1,2] **Jinye Li**,[1] **Zhike Zhang**,[1] **and Jianguo Liu**,[1,2] ***Member, IEEE***

[1]State Key Laboratory on Integrated Optoelectronics, Institute of Semiconductors, Chinese Academy of Sciences, Beijing 100083, China
[2]College of Materials Science and Opto-Electronic Technology, University of Chinese Academy of Sciences, Beijing 100049, China

DOI:10.1109/JPHOT.2020.3041286

Manuscript received October 14, 2020; revised November 20, 2020; accepted November 24, 2020. Date of publication November 30, 2020; date of current version December 31, 2020. This work was supported in part by the National Key R&D Program of China under Grants 2019YFB2203700 and 2018YFB2200504, and in part by the National Natural Science Foundation of China under Grants 61674142 and 62041502. Corresponding author: Jianguo Liu (e-mail: jgliu@semi.ac.cn).

Abstract: A broadband and compact TE-pass/TM-stop polarizer is presented based on hybrid plasmonic grating (HPG) on an x-cut Lithium-Niobate-on-isolator (LNOI) platform. By comprehensively analyzing the effects of metal width on mode effective index, mode similarity, and mode conversion, we demonstrate the structure with a narrow metal layer. The simulation results indicate that the polarizer with a compact length of 9 μm achieves an extinction ratio over 20 dB within the wavelength range from 1470 nm to 1700 nm. The insertion loss is below 2.3 dB in C-band. Furthermore, the polarizer exhibits large fabrication tolerance to current fabrication technology.

Index Terms: Polarizer, hybrid plasmonic grating, LNOI.

1. Introduction

Lithium-Niobate-on-isolator (LNOI) is a promising platform not only because of remarkable electrooptic property, acousto-optic and nonlinear optical properties for integrated photonics as conventional bulk $LiNbO_3$, but also owing to its potential broad application in integrated optics with high index contrast, small footprint compared to bulk $LiNbO_3$ and compatibility with available complementary metal-oxide-semiconductor (CMOS) fabrication process [1]–[3]. However, the performance of the device base on LNOI extremely depends on the polarization due to the anisotropy characteristic like bulk LN. Thus polarizers, which act as a filter to strip off an unexpected polarization, are more fundamental and practical than other polarization handling devices such as polarization splitters and polarization rotators on LNOI platform. The basic principle to design a polarizer is to distinguish one polarization of propagation loss from others. Conventionally, the dielectric-based polarizer has been developed to achieve high extinction ratio (ER) and low insertion loss (IL) [4]–[8]. These polarizers usually utilize shallow-etched waveguide or subwavelength grating waveguide to accomplish large leakage loss. Such polarizers always suffer a large size, complicated structure, and high sensitivity to fabrication. The reported polarizer on LNOI platform based on this strategy reaches an ER as 25 dB with 1-mm-long, which is too long to integrate [8]. Additionally, the

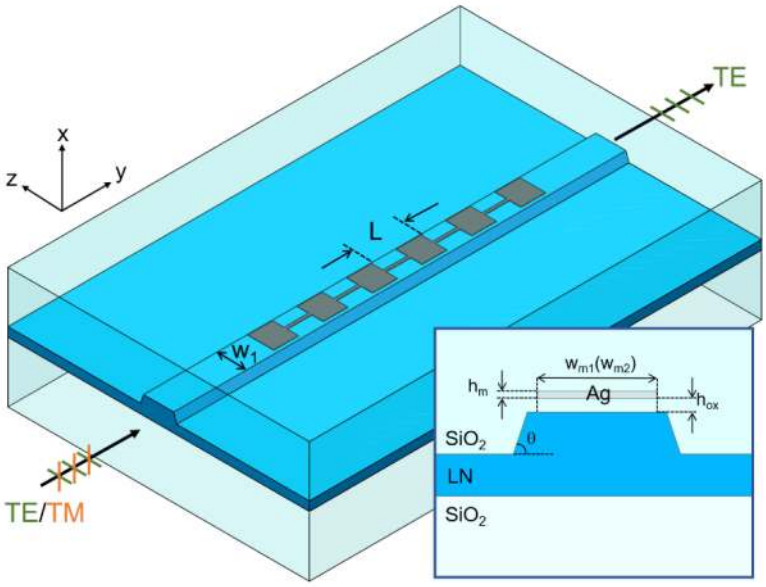

Fig. 1. 3D schematic of the proposed polarizer on LNOI platform and the cross-section of the HPG region. The Si substrate is not shown here for clarity.

fabrication of LN bilayer waveguide is quite challenging, only a few results have been reported [9]. Therefore, alternative schemes of polarizers are in great demand.

Fortunately, surface plasmon polaritons (SPPs) can apply to polarization manipulation benefiting from their natural polarization sensitivity and nanoscale confinement of the electronic field [10]. Various schemes of polarizers have been reported. For instance, the metal-insulator-metal (MIM) structure is introduced to cut off one specific polarization [11]–[13]. The inherent difficulty in using the current planer fabrication process cannot be ignored in these cases. Hybrid plasmonic waveguide (HPW) is another solution to achieve polarizer with high ER, low IR [14], [15], and novel materials [16], [17]. Hybrid plasmonic grating (HPG) is a more practical solution to realize high-performance polarizers with interactions of reflection and mode mismatch [18]–[22]. However, previous works are almost in the situation where the waveguide is strictly single-mode without concerning higher-order modes introduced by the metal grating. As for LNOI platform, the realistic waveguide is multi-mode due to the sloping ridge. Moreover, the effective indices of different modes are in relatively low contrast, increasing the difficulty of polarization control and the device length.

In this paper, we present a wideband and compact TE-pass polarizer by exploiting a narrow HPG on LNOI platform. By comprehensively analyzing the influence of metal width on mode effective index, mode similarity, and mode conversion, the HPG selects a narrower metal width instead of the width fully covering the waveguide. The simulation results indicate that the proposed polarizer achieves an ER over 20 dB within the wavelength from 1470 nm to 1700 nm with a compact length of 9 μm. The IL is below 2.3 dB in C-band. Moreover, the polarizer exhibits large fabrication tolerance.

2. Structure and Analysis

Fig. 1 shows the proposed polarizer based on a 600 nm x-cut y-propagation LNOI platform, involving a cross-section. The device comprises a 2 μm SiO_2 isolation layer on Si substrate, above which is a 300-nm-high ridge LN waveguide with a width of $w_1 = 1$ μm and an inclination angle $\theta = 70°$ with respect to z-axis. Above the LN layer is the Ag waveguide grating. It includes an N periods Ag grating separated from the LN layer by a thin SiO_2 layer with a h_{ox} in height. The main

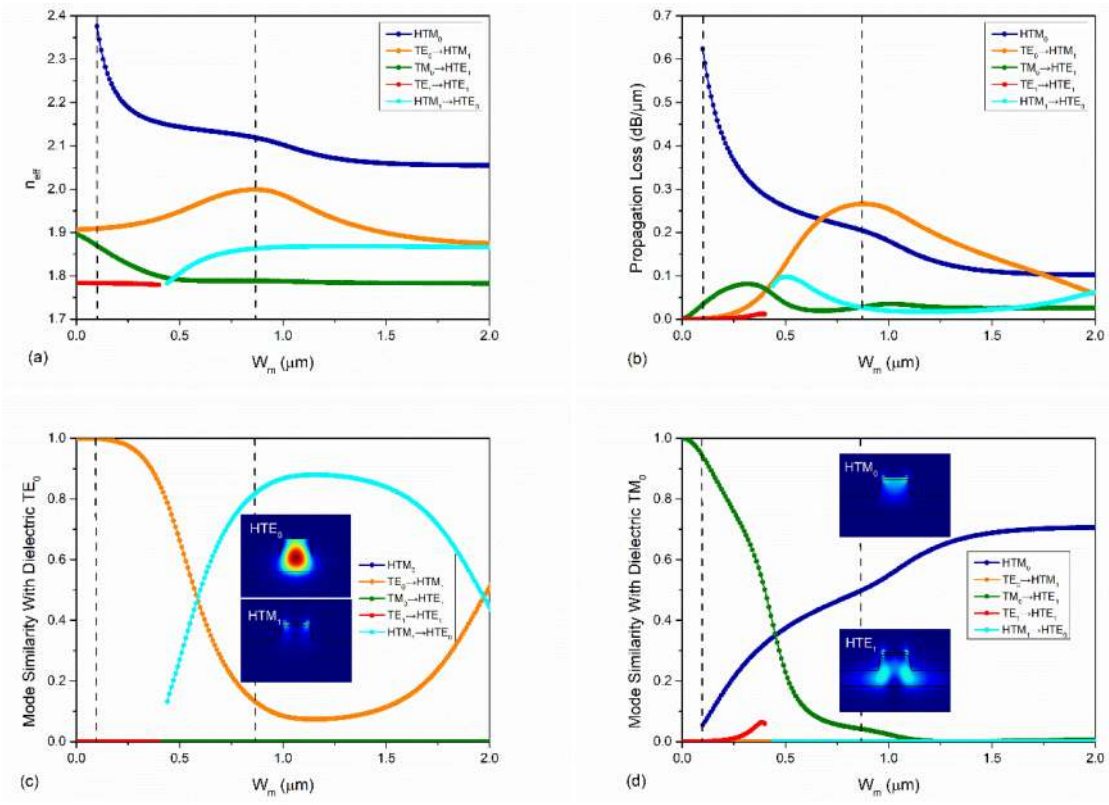

Fig. 2. The (a) n_{eff}, (b) propagation loss, (c) mode similarity with dielectric TE_0 mode, and (d) mode similarity with dielectric TM_0 mode of supported modes as functions of metal width w_m. The dashed lines are at $w_m = 0.1$ μm and $w_m = 0.86$ μm. The insets are magnetic distributions at $w_m = 0.86$ μm. Here, $h_{ox} = 40$ nm and $h_m = 15$ nm.

parameters of the Ag grating are the two widths w_{m1} and w_{m2}, ($w_{m1} > w_{m2}$), height h_m, and duty period L. Here we choose 0.5 as the duty cycle. Noted that the fundamental principle in our design: The loss of TM mode should be much larger than that of TE mode. Owing to the HPG structure, the polarization direction of the TM mode is identical to the excited SPPs mode, inducing a strong reflection and large mode mismatch. On the contrary, the TE mode could pass through the HPG smoothly.

Similar to the conventional Bragg grating, we can define $k = \Delta n_{\text{eff}}/(n_{\text{eff}}L)$ as the coupling coefficient to character the reflection intensity, where Δn_{eff}, n_{eff}, and L are the difference between the mode effective index of the waveguide with different metal width, the mode effective index and the duty period, respectively. Based on former work, a thin h_{ox} of SiO_2 layer will induce not only a large Δn_{eff}, but also a small mode similarity. Here we first set $h_{ox} = 40$ nm and $h_m = 15$ nm as an example. Their specific influence on the performance of the polarizer will be discussed later. Using the finite element method (FEM), we investigate some basic characteristics of the eigenmodes as a function of metal width w_m. The material refractive indices of LN, SiO_2, and Ag at 1550 nm are 2.221 along x and y, 2.138 along z, 1.444, and 0.145+11.438i, respectively [23]. The results are shown in Fig. 2.

As can been seen, though the parameters of the LN waveguide are widely used in reported devices [24]–[26], there still exists a higher dielectric TE_1 mode. Due to the SPPs, the magnetic field is dragged towards the metal layer. When w_m is larger than 0.1 μm, a new hybrid TM_0 mode with a large n_{eff}, and a high propagation loss occurs. The magnetic field of this hybrid TM_0 mode mainly locates beneath the Ag grating initially. This mode cannot be utilized when w_m is small in

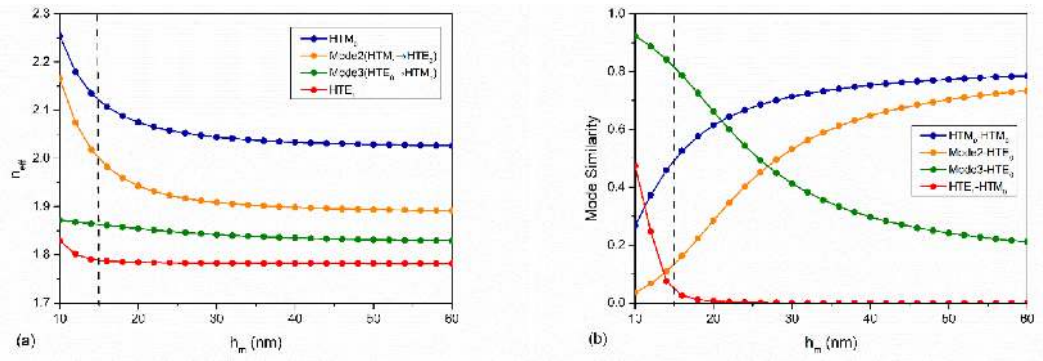

Fig. 3. The (a) n_{eff} and (b) non-zero mode similarity between different modes in HPG region as functions of h_m. Here $h_{ox} = 40$ nm, $w_{m1} = 0.86$ μm, and $w_{m2} = 0.1$ μm.

the polarizer due to large n_{eff} and mode mismatch compared to TM_0. Meanwhile, the initial three modes begin to evolve as w_m increases. The dielectric TE_0 mode gradually converses to hybrid TM_1 mode with a rising n_{eff} and propagation loss. While the TM_0 mode converses to hybrid TE_1 mode as w_m increases with a dropping n_{eff}. This evolution suppresses the original HTE_1 mode and makes it cut off when w_m reaches 0.4 μm. As w_m goes up to 0.44 μm, a new hybrid TM_1 mode appears with a low n_{eff}. Thereafter, the n_{eff}.of the hybrid TM_1 and hybrid TE_0 modes tends to equalize, accounting for the mode conversion between them.

To illustrate the mode evolution clearer, the mode similarity between hybrid modes and dielectric fundamental modes is calculated, the results are shown in Fig. 2(c) and (d). Because the LN ridge is not strictly vertical, there is an extra non-zero mode overlap ratio between hybrid TE_0 and hybrid TM_1, as well as between hybrid TM_0 and hybrid TE_1. Considering the high mode similarity and low Δn_{eff} when w_m is large, a wide metal must be excluded. To avoid such mode conversion, w_{m1} is selected as 0.86 μm, where the $n_{\mathrm{eff},tm1}$ reaches the maximum, as well as the Δn_{eff} reaches the minimum. Given that the descent curve of n_{eff} of TM_0 mode when w_m is small, w_{m2} is selected as 0.1 μm, where a larger Δn_{eff} can be obtained without decreasing the mode similarity between the two TM_0 modes much, marked as the dashed lines. Noted that $n_{\mathrm{eff},TE0,wm1} - n_{\mathrm{eff},TE0,wm2} < n_{\mathrm{eff},TE0,wm1} - n_{\mathrm{eff},TM1,wm2}$, the mode conversion between TE_0 and TM_1 in the HPG region is negligible. Moreover, TM_1 mode is not supported by the dielectric LN ridge waveguide. The generated TM_1 mode will dissipate soon. On the contrary, $n_{\mathrm{eff},TM0,wm1} - n_{\mathrm{eff},TE1,wm2} < n_{\mathrm{eff},TM0,wm1} - n_{\mathrm{eff},TM0,wm2}$, indicating that TM_0 converts to TE_1 inevitably. When it occurs, a large Δn_{eff} between the two modes will also lead to a strong reflection at the interface, not to mention the loss originated from the small mode similarity. The ultimate transmitted wave will be a combination of TM_0 mode and TE_1 mode. Due to n_{eff} and mode similarity change slightly around w_{m1} and w_{m2}, within a deviation of 50 nm, there is perfect robustness of fabrication tolerance for the metal width.

By using the same method, the influence of metal height h_m on n_{eff} and mode similarity is also calculated, as shown in Fig. 3. With h_m going up, the n_{eff} of four modes decrease rapidly first and then gradually become stable, resulting in a small Δn_{eff}. On the other hand, the sequence of hybrid TE_0 mode and hybrid TM_1 exchange as h_m increases. Meanwhile, a mode similarity between TE_1 and TM_0 drops drastically, and that between TM_0 modes increases. If a large h_m is chosen, the TE_0 mode will convert to TM_1 mode on a large scale, resulting in a high IL. Likewise, the performance will be deteriorated, resulting from the mode conversion between TM_0 and TE_1 with a small h_m. Therefore, $h_m = 15$ nm is selected to minimize unnecessary mode conversion as a compromise. Also, a thin metal layer is easy to fabricate by lift-off technology.

Before the overall transmission simulation, the duty period of the HPG should be fixed. According to the condition of Bragg reflection [27]:

$$q\lambda = (neff1 + neff2)Lq \tag{1}$$

where q is the order of the Bragg reflection, λ is set as 1550 nm, L_q is the q-order duty period corresponding to q. A lower q will cause a compact footprint and strong reflection, and yet the fabricating difficulty will increase and the loss of TM mode will decline, suggesting a larger period number N is in need. Hence, we select $q = 2$ and yield $L = 1.66$ μm to balance fabrication feasibility, transmission, and footprint. Additionally, considering that the n_{eff} of TE_0 and TM_0 is quite close, the $n_{\text{eff1}}+n_{\text{eff2}}$ for TE_0 mode of a small w_{m1} is much larger than that of a large one, where the metal totally covers the LN layer. The performance of the polarizer won't be deteriorated by a strong reflection of TE_0 mode.

3. Results and Discussion

3D Finite-Difference-Time-Domain (FDTD) method is carried out to simulate the transmission profile. Here we have set $h_{ox} = 40$ nm, $h_m = 15$ nm, $w_{m1} = 0.86$ μm, and $w_{m2} = 0.1$ μm. In our simulation, the period number is selected as $N = 6$ because it is the smallest N when the minimum transmission of TM_0 mode is lower than -30 dB. First, we investigate the transmission of TE_0 and TM_0 with different duty periods, where the optimum wavelength locates in the C-Band. When $L = 1.64$ μm, the transmission of TM_0 mode is as low as -35 dB at 1535 nm, where the transmission of TE_0 mode is -2.2 dB. The obvious drop of both modes over 1600 nm is due to the metal absorption. The ER keeps over 20 dB within the wavelength range of (1470, 1700) nm. The output wave can be described as a summation of a series of orthogonal eigenmodes $\{E_m, H_m\}$ [19]:

$$\vec{E}out = \sum_m am\vec{E}m,\ \vec{H}out = \sum_m am\vec{H}m \tag{2}$$

where the mode expansion coefficient am can be expressed as follows:

$$am = 0.25 \int (\vec{E}m \times \vec{H}_m^* + \vec{E}_m^* \times \vec{H}m)dS \tag{3}$$

For TM_0 input, we can decompose the output light into TM_0 and TE_1 modes, as Fig. 4(a) shows. TM_0 mode is predominant in the output when the wavelength is shorter than 1500 nm, while TE_1 is leading when the wavelength is larger than 1600 nm, and the output is a superposition of two modes within (1500, 1600) nm. Fortunately, the fraction of TE_1 is too little to influence the performance of other on-chip devices. As for TE_0 input, the output light is complete TE_0 mode without others.

Besides, the reflection spectrums of the polarizer are shown in Fig. 4. Overall, the reflection of TM_0 mode is higher than that for TE_0 mode. For both modes, the reflection is relatively strong in the wavelength range of (1400, 1580) nm because out of a large Δn_{eff} and the plasmonic modes stimulated by reflected lights. The spikes and troughs correspond well between the reflection and transmission function, indicating the reflection plays a major role in this wavelength range. On the contrary, the decrease of reflection accounts for the dominant effect of metal loss resulting from the refractive index of Ag in the bandwidth of (1580, 1800) nm. Furthermore, the power propagation profile is depicted. It can be seen that the TM_0 mode attenuated rapidly, and the mode conversion to TE_1 at the interface of the HPG. While TE_0 mode passes through the HPG with little loss and reflection. The following discussion will be based on $L = 1.64$ μm.

Here we define ER and IL as ER $= -10\log(P_{TM}/P_{TE})$ and IL $= -10\log(P_{TE}/P_{in})$ to evaluate the performance of the proposed polarizer, where P_{TM}, P_{TE}, and P_{in} are the output power when TM mode injected, TE mode injected, and the input power. It is worth noting that the P_{TM} contains parts of TE_1 mode.

The height of the oxide layer, h_{ox}, also has a significate impact on the performance of the polarizer. With the accuracy of the sputtering into consideration, the sensitivity to the h_{ox} should be carried out. As shown in Fig. 5, the optimum wavelength goes down when h_{ox} increases. The ER reaches the highest to 32 dB as $h_{ox} = 40$ nm and stays higher than 15 dB within our simulated

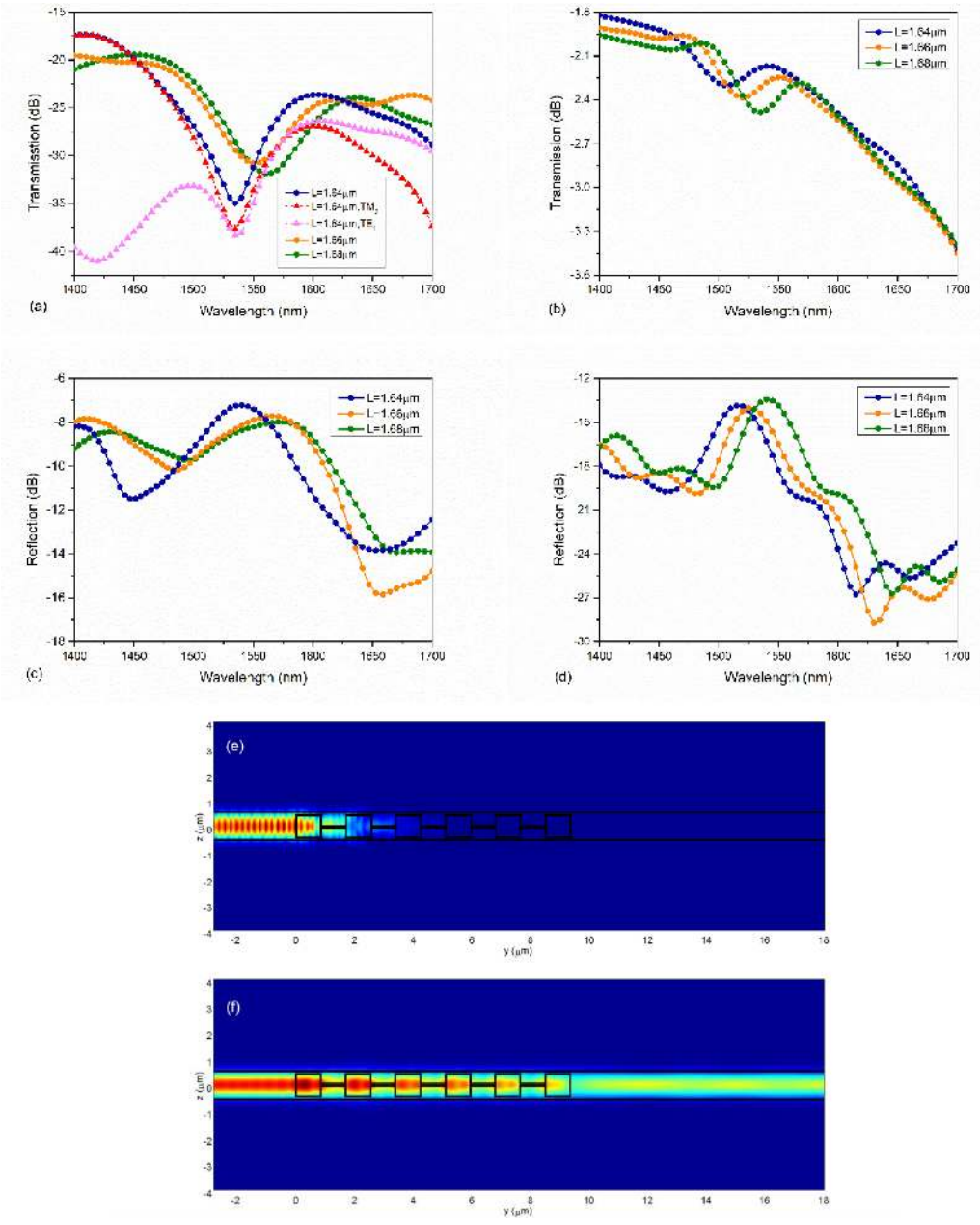

Fig. 4. Simulated (a) transmission of TM, (b) transmission of TE, (c) reflection of TM, (d) reflection of TE with different duty periods L as functions of wavelength. (e) and (f) are the power propagation profile of the proposed polarizer for TM and TE mode at $\lambda = 1535$ nm, here $L = 1.64$ μm.

bandwidth. On the other hand, there is a positive correlation between IL and hox. The IL in C-band is still lower than 3 dB when h_{ox} is within (25, 55) nm. Whereas the increasing IR with smaller h_{ox}, the oxide layer should be deposited cautiously.

It is not easy to manipulate the profile of the LN ridge waveguide precisely during the sophisticated fabrication process. The tolerance of the polarizer to the LN layer is investigated. The waveguide width, w_1, is closely related to the mask and etching conditions. There is usually a slight difference between the actual width and the desired one. A larger w_1, which is easier to fabricate,

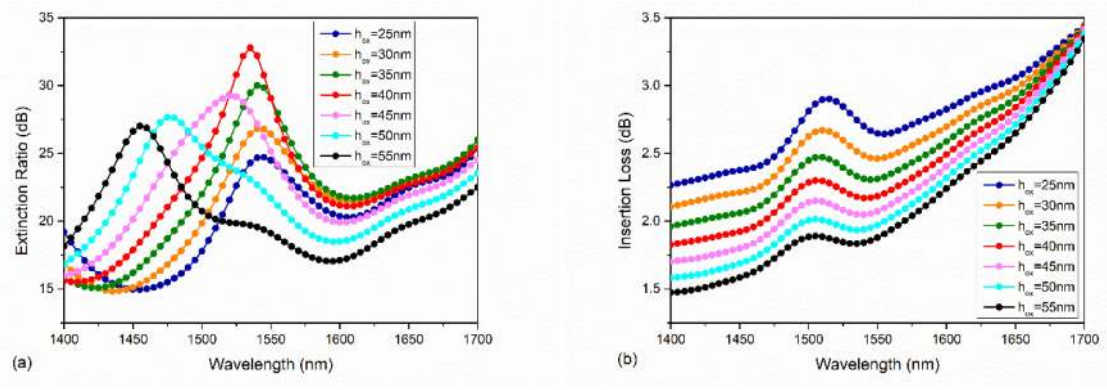

Fig. 5. The (a) ERs and (b) ILs of the proposed polarizer as functions of wavelength with different h_{ox}.

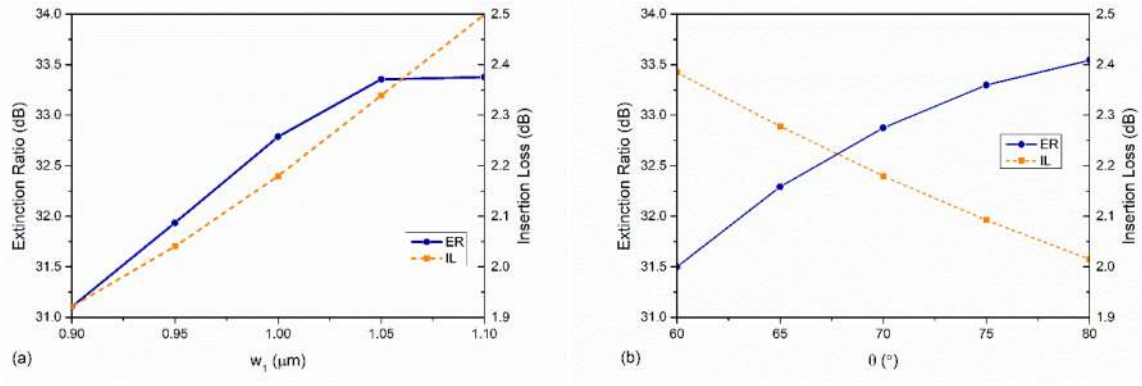

Fig. 6. ERs and ILs as functions of (a) waveguide width w_1 and (b) inclination angle θ of the LN layer of the proposed polarizer.

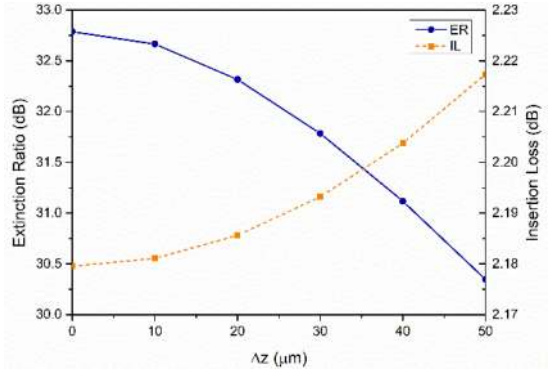

Fig. 7. ER and IL as functions of misalignment along z axis Δz.

will raise the mode mismatch for both modes, resulting in larger ER and IL. But it supports more eigenmodes simultaneously. Since the simulated results at different w_1 are nearly parallel to each other, Fig. 6 depicts the ER and IL at 1535 nm for simplicity. The ER always exceeds 31 dB, while the IL has a liner ascent to 2.5 dB when w_1 reached 1.1 μm. The performance is acceptable as w_1 varies.

In our initial assumption, the inclination angle of the LN ridge is 70°, a reasonable angle for current fabrication technology. Nonetheless, the inclination angle is also hard to anticipate since

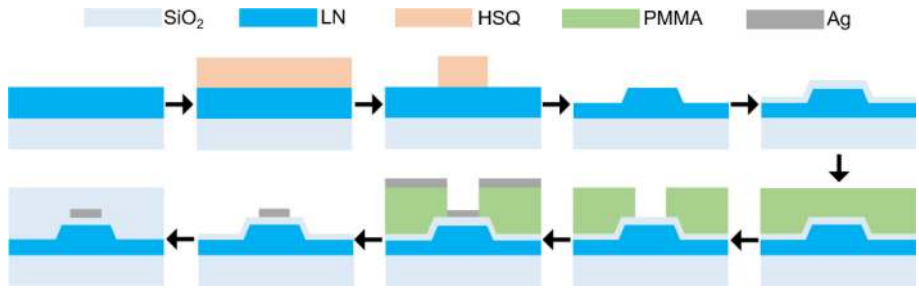

Fig. 8. The fabrication process of the proposed polarizer.

the ridge surface tends to redeposition of LiF during the process when LN is milled by a mix of fluorine and Ar plasma [28], [29]. Therefore, the effect of the inclination angle on the polarizer is considered. Here the θ varies from 60° to 80°. It can be concluded that the performance becomes higher when θ gets larger, and the ER keeps over 31.5 dB while the IL keeps below 2.4 dB. This is because when the ridge gets steeper, both the TE and TM mode distributions are more uniform along the x-axis, leaving non-orthogonal electrical components less around the slope. Thus, the effect of HPG is stronger for a better momentum match. Nevertheless, the performance of the polarizer does not deteriorate severely when θ varies.

During the sputtering of the metal, the deviation along the y-axis can be erased. But the misalignment of the metal and the center of the LN ridge is inevitable the overlay of electron beam lithography (EBL). When such asymmetric hybrid structure occurs, TE_0 and TM_0 modes will rotate to each other because of mode-interference [30]–[32]. The influence of the z misalignment, $\triangle z$ is calculated as well. Considering this rotation, the output light is a combination of TE_0, TM_0, and TE_1 mode no matter what the input mode is. Fortunately, owing to the compact size of the polarizer, the performance of the polarizer hardly degenerates when $\triangle z$ is below 50 nm, a quite large fabrication error. The ER can stay higher than 30.5 dB while the IL only increases 0.04 dB. The variation of ER and IL represents the rotation fraction when TE_0 or TM_0 mode is injected, respectively. The slight fraction of conversed modes, less than 10^{-2}, will not affect the subsequent devices.

4. Fabrication Feasibility

The fabrication process is depicted in Fig. 8. The negative tone resist, hydrogen silsesquioxane (HSQ), is select as the mask, followed by EBL to pattern the waveguide. The LN layer is etched with CHF_3 and Ar plasma in an inductively coupled plasma (ICP) system. The SiO_2 thin spacer layer is formed by plasma-enhanced chemical vapor deposition (PECVD). Then PMMA, a positive resist is spin-coated. After the second EBL process, the 15 nm-thick Ag layer is sputtered. By proper lift-off process, the HPG region is fabricated. Finally, the SiO_2 cladding is deposited by PECVD.

5. Conclusion

In summary, a broadband and compact TE-pass polarizer on LNOI platform is theoretically demonstrated. A comprehensive simulation has been conducted to analyze the influence of metal width on mode effective index, mode similarity, and mode conversion. We select two narrower metal width $w_{m1} = 0.86$ μm and $w_{m2} = 0.1$ μm in the HPG instead of the wider one fully covering the waveguide to enhance the performance. For a 9-μm-long polarizer, the simulation results indicate that it achieves an ER from 15 to 33 dB within the wavelength of (1400, 1700) nm. The corresponding IL is from 1.8 to 3.4 dB. Furthermore, it exhibits a large fabrication tolerance to the metal layer as well as the LN layer. The high performance and compact size will make the proposed polarizer a potential choice for integrated photonics on LNOI platform.

References

[1] R. S. Weis and T. K. Gaylord, "Lithium niobate: Summary of physical properties and crystal structure," *Appl. Phys. A*, vol. 37, no. 4, pp. 191–203, Aug. 1985.

[2] G. Poberaj, H. Hu, W. Sohler, and P. Günter, "Lithium niobate on insulator (LNOI) for micro-photonic devices," *Laser Photon. Rev.*, vol. 6, no. 4, pp. 488–503, Jul. 2012.

[3] A. Boes, B. Corcoran, L. Chang, J. Bowers, and A. Mitchell, "Status and potential of lithium niobate on insulator (LNOI) for photonic integrated circuits," *Laser Photon. Rev.*, vol. 12, no. 4, 2018, Art. no. 1700256.

[4] D. Dai, Z. Wang, N. Julian, and J. E. Bowers, "Compact broadband polarizer based on shallowly-etched silicon-on-insulator ridge optical waveguides," *Opt. Exp.*, vol. 18, no. 26, pp. 27404–27415, Dec. 2010.

[5] Q. Wang and S.-T. Ho, "Ultracompact TM-pass silicon nanophotonic waveguide polarizer and design," *IEEE Photon. J.*, vol. 2, no. 1, Feb. 2010.

[6] X. Guan, P. Chen, S. Chen, P. Xu, Y. Shi, and D. Dai, "Low-loss ultracompact transverse-magnetic-pass polarizer with a silicon subwavelength grating waveguide," *Opt. Lett.*, vol. 39, no. 15, pp. 4514–4517, Aug. 2014.

[7] Y. Xiong, D.-X. Xu, J. H. Schmid, P. Cheben, and W. N. Ye, "High extinction ratio and broadband silicon TE pass polarizer using subwavelength grating index engineering," *IEEE Photon. J.*, vol. 7, no. 5, Oct. 2015, Art. no. 7802107.

[8] E. Saitoh, Y. Kawaguchi, K. Saitoh, and M. Koshiba, "TE/TM-pass polarizer based on lithium niobate on insulator ridge waveguide," *IEEE Photon. J.*, vol. 5, no. 2, Apr. 2013, Art. no. 6600610.

[9] L. He, M. Zhang, A. Shams-Ansari, R. Zhu, C. Wang, and M. Lončar, "Low-loss fiber-to-chip interface for lithium niobate photonic integrated circuits," *Opt. Lett.*, vol. 44, no. 9, pp. 2314–2317, May 2019.

[10] D. K. Gramotnev and S. I. Bozhevolnyi, "Plasmonics beyond the diffraction limit," *Nat. Photon.*, vol. 4, no. 2, pp. 83–91, Feb. 2010.

[11] T. K. Ng, M. Z. M. Khan, A. Al-Jabr, and B. S. Ooi, "Analysis of CMOS compatible Cu-based TM-pass optical polarizer," *IEEE Photon. Technol. Lett.*, vol. 24, no. 9, pp. 724–726, Feb. 2012.

[12] Y. Xu and J. Xiao, "A compact TE-pass polarizer for silicon-based slot waveguides," *IEEE Photon. Technol. Lett.*, vol. 27, no. 19, pp. 2071–2074, Oct. 2015.

[13] X. Sun, M. Z. Alam, S. J. Wagner, J. S. Aitchison, and M. Mojahedi, "Experimental demonstration of a hybrid plasmonic transverse electric pass polarizer for a silicon-on-insulator platform," *Opt. Lett.*, vol. 37, no. 23, pp. 4814–4816, Dec. 2012.

[14] Z. Ying, G. Wang, X. Zhang, Y. Huang, H.-P. Ho, and Y. Zhang, "Ultracompact TE-pass polarizer based on a hybrid plasmonic waveguide," *IEEE Photon. Technol. Lett.*, vol. 27, no. 2, pp. 201–204, Jan. 2015.

[15] M. Alam, J. S. Aitchsion, and M. Mojahedi, "Compact hybrid TM-pass polarizer for silicon-on-insulator platform," *Appl. Opt.*, vol. 50, no. 15, pp. 2294–2298, May 2011.

[16] L. Sánchez, S. Lechago, and P. Sanchis, "Ultra-compact TE and TM pass polarizers based on vanadium dioxide on silicon," *Opt. Lett.*, vol. 40, no. 7, pp. 1452–1455, Apr. 2015.

[17] P. Xu, Y. Lu, Z. Yu, and S. Dai, "Ultra-compact active TE and TM pass polarizers based on $Ge_2Sb_2Te_5$ in silicon waveguide," *IEEE Photon. Technol. Lett.*, vol. 28, no. 23, pp. 2697–2700, Dec. 2016.

[18] Z. Ying, G. Wang, X. Zhang, Y. Huang, H.-P. Ho, and Y. Zhang, "Ultracompact TE-pass polarizer based on a hybrid plasmonic waveguide," *IEEE Photon. Technol. Lett.*, vol. 27, no. 2, pp. 201–204, Jan. 2015.

[19] B. Bai, L. Liu, R. Chen, and Z. Zhou, "Low loss, compact TM-Pass polarizer based on hybrid plasmonic grating," *IEEE Photon. Technol. Lett.*, vol. 29, no. 7, pp. 607–610, Apr. 2017.

[20] B. Bai, F. Yang, and Z. Zhou, "Demonstration of an on-chip TE-pass polarizer using a silicon hybrid plasmonic grating," *Photon. Res.*, vol. 7, no. 3, pp. 289–293, Mar. 2019.

[21] W. Yu, S. Dai, Q. Zhao, J. Li, and J. Liu, "Wideband and compact TM-pass polarizer based on hybrid plasmonic grating in LNOI," *Opt. Exp.*, vol. 27, no. 24, pp. 34857–34863, Nov. 2019.

[22] Q. Zhao, W. Yu, Y. Zhao, S. Dai, and J. Liu, "TiO_2-based compact TM-pass polarizer at visible wavelengths with ultra-low power loss," *Opt. Commun.*, vol. 475, Nov. 2020, Art. no. 126282.

[23] P. B. Johnson and R. W. Christy, "Optical constants of the noble metals," *Phys. Rev. B*, vol. 6, no. 12, pp. 4370–4379, Dec. 1972.

[24] M. Zhang, C. Wang, R. Cheng, A. Shams-Ansari, and M. Lončar, "Monolithic ultra-high-Q lithium niobate microring resonator," *Optica*, vol. 4, no. 12, pp. 1536–1537, Dec. 2018.

[25] M. He *et al.*, "High-performance hybrid silicon and lithium niobate Mach-Zehnder modulators for 100 gbit s-1 and beyond," *Nat. Photon.*, vol. 13, no. 5, pp. 359–364, May 2019.

[26] B. Desiatov, A. Shams-Ansari, M. Zhang, C. Wang, and M. Lončar, "Ultra-low loss integrated visible photonics using thin-film lithium niobate," *Optica*, vol. 6, no. 3, pp. 380–384, Mar. 2019.

[27] P. A. Snow, E. K. Squire, P. S. J. Russell, and L. T. Canham, "Vapor sensing using the optical properties of porous silicon Bragg mirrors," *J. Appl. Phys.*, vol. 86, no. 4, pp. 1781–1784, Aug. 1999.

[28] H. Hu, R. Ricken, W. Sohler, and R. B. Wehrspohn, "Lithium niobate ridge waveguides fabricated by wet etching," *IEEE Photon. Technol. Lett.*, vol. 19, no. 6, pp. 417–419, Feb. 2007.

[29] I. Krasnokutska, J. J. Tambasco, X. Li, and A. Peruzzo, "Ultra-low loss photonic circuits in lithium niobate on insulator," *Opt. Exp.*, vol. 26, no. 2, pp. 897–904, Jan. 2018.

[30] L. Gao, Y. Huo, J. S. Harris, and Z. Zhou, "Ultra-compact and low-loss polarization rotator based on asymmetric hybrid plasmonic waveguide," *IEEE Photon. Technol. Lett.*, vol. 25, no. 21, pp. 2081–2084, Nov. 2013.

[31] Y. C. and T. Y., "Photonic-Quasi-TE-to-hybrid-plasmonic-TM polarization mode converter," *J. Lightw. Technol.*, vol. 33, no. 20, pp. 4261–4267, Oct. 2015.

[32] Y. Xu, J. Xiao, and X. Sun, "A compact hybrid plasmonic polarization rotator for silicon-based slot waveguides," *IEEE Photon. Technol. Lett.*, vol. 26, no. 16, pp. 1609–1612, Aug. 2014.